Earthq Sci (2016) 29(2):117–125
DOI 10.1007/s11589-016-0147-2

RESEARCH PAPER

Three-dimensional admittance analysis of lithospheric elastic thickness over the Louisville Ridge

Minzhang Hu · Hui Li · Chongyang Shen · Lelin Xing · Hongtao Hao

Received: 30 September 2015 / Accepted: 17 February 2016 / Published online: 23 April 2016

Abstract Using bathymetry and altimetric gravity anomalies, a 1° × 1° lithospheric effective elastic thickness (T_e) model over the Louisville Ridge and its adjacent regions is calculated using the moving window admittance technique. For comparison, three bathymetry models are used: general bathymetric charts of the oceans, SIO V15.1, and BAT_VGG. The results show that BAT_VGG is more suitable for calculating T_e than the other two models. T_e along the Louisville Ridge was re-evaluated. The southeast of the ridge has a medium T_e of 10–20 km, while T_e increases dramatically seaward of the Tonga-Kermadec trench as a result of the collision of the Pacific and Indo-Australian plates.

Keywords Three-dimensional admittance analysis · Lithospheric effective elastic thickness · Bathymetry · Gravity · Louisville Ridge

1 Introduction

Although, as a seamount chain, it is exceeded in size only by the Hawaiian-Emperor Chain, little is known about the tectonic settings of the Louisville Ridge because of its remote location. The effective elastic thickness of the lithosphere (T_e) is a fundamental parameter that is sensitive to the tectonic settings of a submarine feature. There have been few attempts at calculating the T_e beneath features over the Louisville Ridge (Cazenave and Dominh 1984; Watts et al. 1988; Lyons et al. 2000)—probably because it has been surveyed by few ships, and high-accuracy depth and gravity data are sparse.

Constraining with sparsely distributed seas at geoid profiles, Cazenave and Dominh (1984) employed a three-dimensional (3D) forward modeling method to estimate T_e over the Louisville Ridge. The geoid heights were calculated for different values of T_e using bathymetric data. T_e was recovered by minimizing the misfits between modeled geoid heights and seas at geoid profiles. The resolutions of both the geoid and the bathymetry that they used were relatively low. Watts et al. (1988) estimated T_e over the ridge systematically using high-resolution ship bathymetry and gravity profiles perpendicular to the ridge. However, these two studies gave contradictory results. According to Cazenave and Dominh (1984), T_e increased from southeast to northwest, while Watts et al. (1988) found the opposite trend. Lyons et al. (2000) tried to reconcile these results and introduced a 3D "bathymetry-predicting" method to estimate T_e. In this method, the bathymetry around a seamount is predicted using high-resolution gravity anomalies derived from Geosat altimetric data for different T_e. The predicted bathymetry is then compared with in situ ship soundings. T_e is then recovered by minimizing the differences between the ship soundings and the predicted bathymetry. The results of Lyons et al. (2000) tend to agree with those of Cazenave and Dominh (1984) with respect to trend, showing increasing values from southeast to northwest.

The resolution and accuracy of altimetric gravity anomalies have improved dramatically in recent years (Sandwell and Smith 2009). Kalnins and Watts (2009) introduced the moving window admittance technique (MWAT) to determine the spatial variation of T_e in the western Pacific, based on general bathymetric charts of the

M. Hu · H. Li (✉) · C. Shen · L. Xing · H. Hao
Key Laboratory of Earthquake Geodesy, Institute of Seismology, China Earthquake Administration, 40 Hongshan Celu, Wuhan, China
e-mail: lihuieq@163.com

oceans (GEBCOs) and altimetric gravity anomaly data (SIO, version V16.1). In this method, T_e is estimated by 3D spectral analysis for different window sizes (400 km × 400 km to 1400 km × 1400 km), and the final T_e is the weighted mean of the results for different window sizes. GEBCO is the only grid that is not based on satellite altimetry data, but its accuracy is very low and it has the problem of "terrace" (Smith 1993).

In this study, using the MWAT method, a 1° × 1° T_e model over the Louisville Ridge is re-calculated, with a new bathymetry model based on vertical gravity gradient anomaly data and ship soundings (BAT_VGG) (Hu et al. 2014). For comparison, GEBCO and the SIO V15.1 model are also used. The results show that BAT_VGG is superior to GEBCO and SIO V15.1 for estimating T_e. The results are discussed in detail. The correlation between T_e and the age of the lithosphere at the time of loading is re-evaluated based on our estimates of T_e and the newest seamount ages from Clouard and Bonneville (2005) and Koppers et al. (2004, 2011) along the Louisville Ridge. The bathymetry and locations of seamount age samples are shown in Plate 1.

2 Theory

The theoretical basis for estimating T_e is the flexural isostatic model (Watts 2001). Figure 1 illustrates a simple flexural crust model, in which $h(x)$ is the seafloor topography and $r(x)$ is the flexure of the Mohorovičić discontinuity (Moho) introduced by the seamount loading. The parameters of this simple model are summarized in Table 1.

In the frequency domain, according to the flexural isostatic model, the flexure of the Mohocan be obtained as

$$R(k) = -H(k)\frac{(\rho_c - \rho_w)}{(\rho_m - \rho_c)}\Phi_e(k). \quad (1)$$

Here $R(k)$ is the Fourier transform of $r(x)$, $H(k)$ is the Fourier transform of $h(x)$, $k = 2\pi/\lambda$ is the wavenumber, λ is the wavelength, ρ_m, ρ_c, and ρ_w are the densities of mantle, crust, and seawater, respectively, and $\Phi_e(k)$ is the flexural

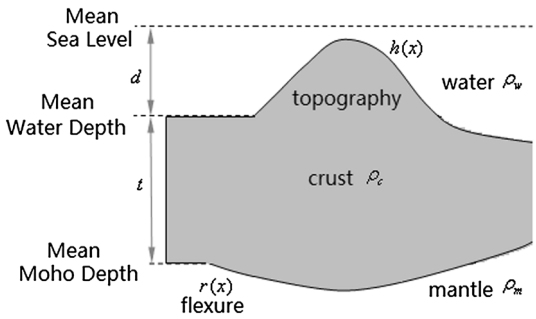

Fig. 1 A simple flexural isostatic model

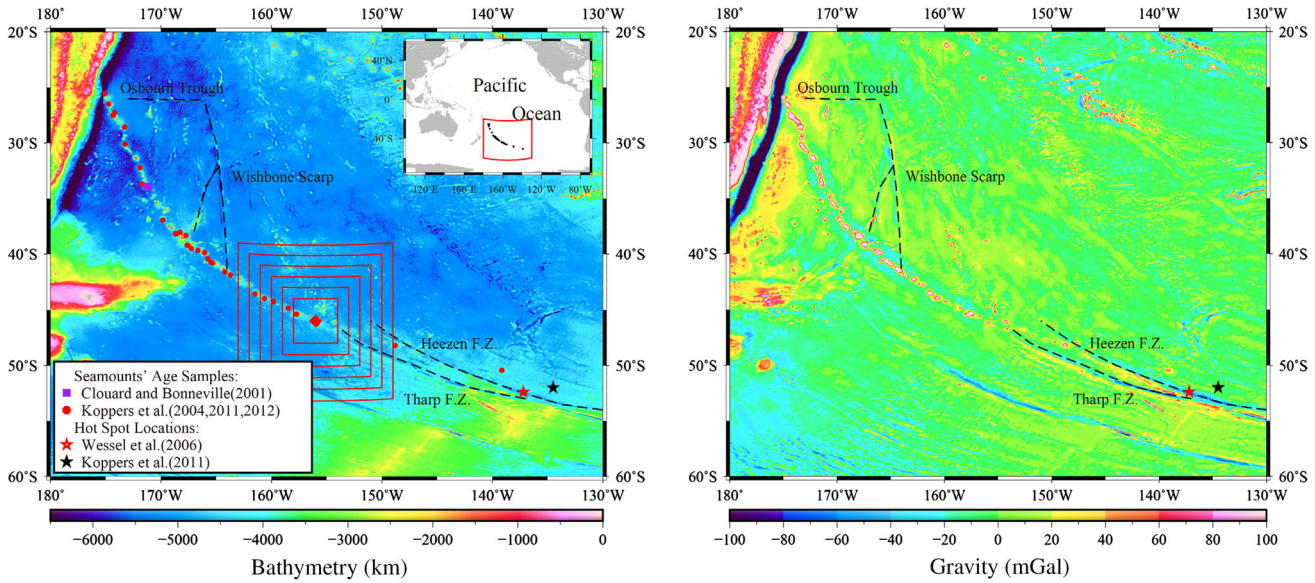

Plate 1 Bathymetry and free-air gravity anomalies over the Louisville Ridge system, southwest Pacific. Bathymetry data are taken from Hu et al. (2014) (BAT_VGG). The gravity anomalies are taken from SIO V20.1. *Red dots* and *purple square* denote sample locations from Clouard and Bonneville (2005) and Koppers et al. (2004, 2011, 2012), respectively, and the ages of these samples are shown in Table 5. *Red star* indicates the location of a hot-spot given by Wessel et al. (2006), and the *black star* shows the location from Koppers et al. (2011). *Red diamond* shows the location of the experiment described in Sect. 3, and the *red boxes* around it denote the extent of the data (the size of the windows) used for estimating T_e by the MWAT method

response function of the lithosphere, given by Walcott (1976)

$$\Phi_e(k) = \left[\frac{Dk^4}{(\rho_m - \rho_c)g} + 1\right]^{-1}, \quad (2)$$

where g is the average acceleration due to gravity and $D = ET_e^3/[12(1-\upsilon^2)]$ is the flexural rigidity of the lithosphere (E is Young's modulus and υ is Poisson's ratio). Combining Eq. (4) in Parker (1973) with Eqs. (1) and (2), the gravity anomaly introduced by seafloor topography and the compensation mass is given by

$$\Delta G(k) = 2\pi G(\rho_c - \rho_w)e^{-kd}\left[1 - \Phi_e(k)e^{-kt}\right] \times \left\{H(k) + \sum_{n=2}^{\infty}\frac{k^{n-1}}{n!}F[h^n(x)]\right\}, \quad (3)$$

where $\Delta G(k)$ is the gravity anomaly in the frequency domain, G is the universal gravitational constant, d is the mean water depth, t is the mean crustal thickness, and F indicates the Fourier transform. Discarding higher-order terms ($n \geq 2$) in Eq. (3), the admittance relationship between seafloor topography and gravity anomaly data is

$$G(k) = 2\pi G(\rho_c - \rho_w)e^{-kd}\left[1 - \Phi_e(k)e^{-kt}\right]H(k). \quad (4)$$

Thus, we obtain the theoretical admittance, as given by Watts (2001):

$$Z(k) = 2\pi G(\rho_c - \rho_w)e^{-kd}\left[1 - \Phi_e(k)e^{-kt}\right]. \quad (5)$$

The theoretical admittance curves are shown in Fig. 2 for different parameter values.

According to Fig. 2, at wavelengths shorter than 50 km, the theoretical admittance does not change significantly for different T_e, since the topography is uncompensated at these wavelengths. The uncompensated theoretical admittance ($Z_{uncom}(k)$, shown by the thick blue line in Fig. 2) is given by

$$Z_{uncom}(k) = 2\pi G(\rho_c - \rho_w)e^{-kd}. \quad (6)$$

Table 1 Summary of parameters assumed for the simple flexural isostatic model

Parameters	Symbols	Values
Density of seawater	ρ_w	1030 kg/m^3
Density of crust	ρ_c	2800 kg/m^3
Density of mantle	ρ_m	3350 kg/m^3
Mean crustal thickness	t	6.5 km
Young's modulus	E	10^{11} N/m^2
Poisson's ratio	υ	0.25

3 Method

The MWAT method introduced by Kalnins and Watts (2009) was used in this study. T_e is estimated by 3D spectral analysis for different window sizes (400 km × 400 km to 1400 km × 1400 km). The final T_e is computed from a weighted mean of the results for different window sizes.

As an example, over the selected point as shown in Plate 1 (the red diamond at location 156°W, 46°S), the compensated and uncompensated theoretical admittances can be calculated using Eqs. (5) and (6). The observed admittance $Z'(k)$ can be determined from observed gravity anomaly data, $\Delta G'(k)$, and the seafloor topography model $B(k)$ as (McNutt 1979)

$$Z'(k) = \frac{\langle G'(k)\cdot B^*(k)\rangle}{\langle B(k)\cdot B^*(k)\rangle}, \quad (7)$$

where * denotes the complex conjugate, and $\langle\cdot\rangle$ indicates annular averaging of the spectral estimates. T_e can be established by minimizing the root mean square (RMS) misfits between the observed and theoretical admittances. We calculated T_e in two steps. First, in the 20–50 km wave band, the uncompensated theoretical admittance is calculated using Eq. (6) for different ρ_c (2300–2900 kg/cm^3) and d (mean model depth ± 500 m). The values of ρ_c and d can be recovered area by area by fitting the theoretical and observed admittances. Second, at wavelengths longer than 50 km, using the recovered ρ_c and d, the theoretical admittance can be calculated using Eq. (5) for different T_e. We obtain the optimal T_e when the RMS misfit is minimized.

Over the selected point (Plate 1, red diamond), for a window size of 10° × 10°, using the 3D spectral analysis method, the best estimated T_e is as shown in Fig. 3. According to Fig. 3, physically plausible values for ρ_c and d can be recovered, and the best fitted T_e for the selected

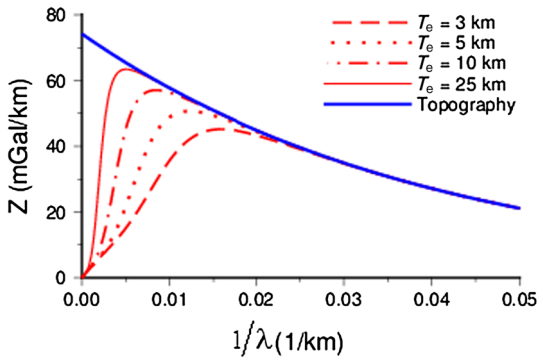

Fig. 2 Theoretical admittance curves for T_e = 3, 5, 10, and 25 km. *Thick blue line* denotes the uncompensated admittance between bathymetry and the gravity anomaly

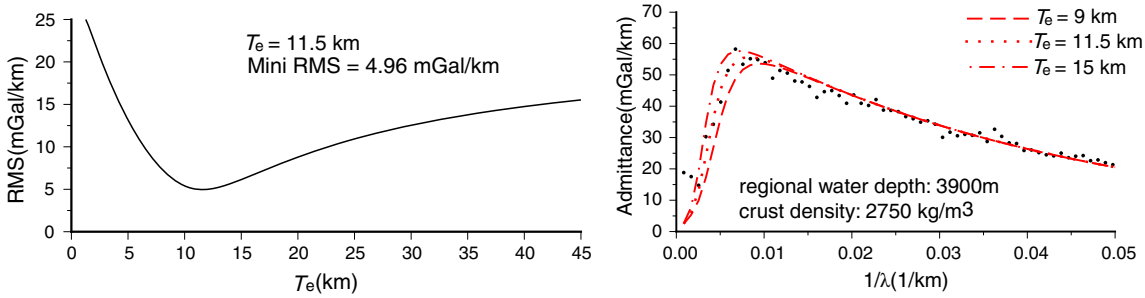

Fig. 3 The RMS misfit between theoretical and observed admittances for different T_e (*left*), and comparison of theoretical and observed admittances (*right*). *Black dots* denote the observed admittance, and the *red dashed*, *dotted*, and *dot-dashed lines* indicate the theoretical admittances for $T_e = 9$, 11.5, and 15 km, respectively. The observed admittance is calculated using the software package gravfft developed by Luis and Neves (2006)

point is 11.5 km, while the minimal RMS misfit between the observed and theoretical admittances is 5.1 mGal/km.

With the MWAT method, six windows from 400 km × 400 km to 1400 km × 1400 km are used to estimate T_e. For different window sizes, different spectral samples are used by gravfft to calculate the observed admittance. At the selected point (156°W, 46°S), the result is as shown in Fig. 4 and Table 2.

4 Data and results

4.1 Data

In order to calculate T_e with the MWAT method, seafloor topography and gravity anomaly grids are needed. In this study, we use gravity anomaly data from the Scripps Institution of Oceanography, University of California, San Diego (SIO version V20.1), which are derived from satellite altimetric observations (Sandwell and Smith 2009). Three kinds of bathymetry model, GEBCO, SIO V15.1, and BAT_VGG, are used, in order to test which is the best. GEBCO is the only grid that is not based on satellite altimetry data. It is a 1-min grid prepared from bathymetric contours of the world's oceans and was originally available as a series of paper maps at 1:10 million scale and later as digital contours in the GEBCO Digital Atlas. These maps were contoured at 500-m depth intervals, by hand, from digital and analog ship soundings (Marks and Smith 2006). SIO V15.1 was released by the SIO and was derived from ship soundings and satellite altimetric gravity anomalies (Smith and Sandwell 1994). BAT_VGG was created using ship soundings and vertical gravity gradient anomalies (Hu et al. 2014). Both GEBCO and the SIO V15.1 model have been used to estimate oceanic lithospheric T_e in some published papers (Kalnins and Watts 2009; Luis and Neves 2006). The accuracy of GEBCO is significantly lower than that of SIO V15.1. At the same time, however, some authors may doubt the results if SIO V15.1 is used to recover T_e using the 3D spectral analysis technique, since the bathymetry is derived from gravity anomaly data in the 15–160 km wave band.

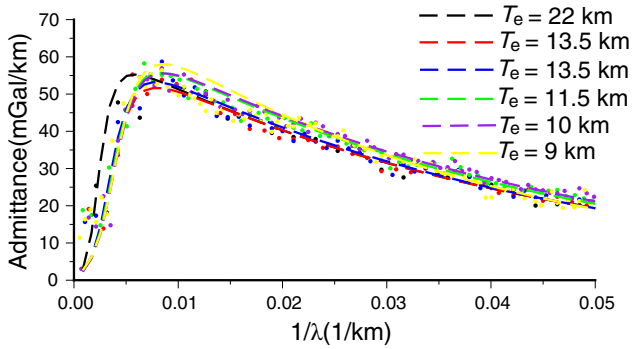

Fig. 4 Best fitted T_e for different window sizes. *Black*, *red*, *blue*, *green*, *purple*, and *yellow dashed lines* indicate the results for window sizes from 400 km × 400 km to 1400 km × 1400 km, respectively

4.2 Results

In this study, a 1° × 1° T_e model is calculated over the Louisville Ridge and the adjacent regions (180°E–230°E,

Table 2 Estimated T_e and spectral samples of the observed admittance for different window sizes

Window	4° × 4°	6° × 6°	8° × 8°	10° × 10°	12° × 12°	14° × 14°
T_e (km)	22.0	13.5	13.5	11.5	10.0	9.5
Samples	23	35	47	59	70	94

T_e over the point (156°W, 46°S) is finally obtained as the weighted mean of the six results in the table. The spectral samples are taken as the weights, and the weighted T_e is about 11.8 km

60°S–20°S). T_e is estimated on 2091 grid nodes. A histogram of the distribution of the minimal RMS misfits between observed and theoretical admittances is shown in Fig. 5. The statistics of the recovered crustal density and minimal RMS misfits are given in Table 3.

In Table 3, when using BAT_VGG to calculate T_e, the mean of the recovered crustal density is 2.704 g/cm^3, which is consistent with the mean crustal density from CRUST2.0 (about 2.772 g/cm^3), the mean of the minimal RMS misfits is 5.834 mGal/km, 32.042 % of the RMS misfits are not larger than 5 mGal/km, and more than 99 % of the RMS misfits are not larger than 10 mGal/km. These results show that BAT_VGG is superior to the other two models when calculating T_e using the MWAT method.

Frequency distribution histograms of T_e are shown in Fig. 6 for the different bathymetry models used. According to Fig. 6c, most of the values of T_e over the Louisville Ridge and its adjacent regions are less than 15 km.

T_e estimated using BAT_VGG is shown in Fig. 7, from which it can be seen that T_e lies in the range 0–50 km, with a mean of 11.924 km and a standard deviation of 10.174 km. In the northwest of the study area, the estimated T_e is clearly larger than elsewhere. The Louisville Ridge system has a medium value of T_e (10–20 km). In general, T_e over the basins both at the northeast and the southwest of the ridge is less than 10 km.

In the study area, the T_e of the lithosphere under 609 seamounts was estimated by Watts et al. (2006) using a bathymetry predicting method. The differences between their results and those of this study are shown in Fig. 8. Most of the absolute differences are less than 10 km, with a mean of −1.6 km and a standard deviation of 4.5 km.

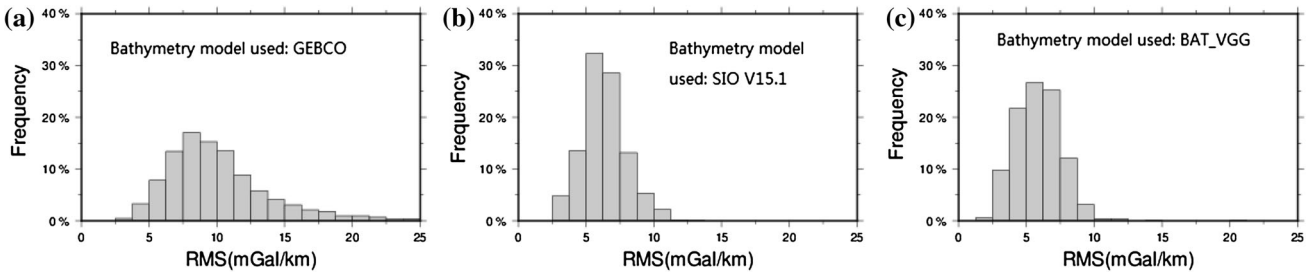

Fig. 5 Frequency distribution of minimal RMS misfits between observed and theoretical admittances when using **a** GEBCO, **b** SIO V15.1, and **c** BAT_VGG

Table 3 Statistics of recovered crustal density and minimal RMS misfits between observed and theoretical admittances for different bathymetry models

Bathymetry models	Mean (SD) of recovered crustal density (g/cm^3)	Mean (SD) of minima misfit between observed and theoretical admittance (mGal/km)	Percentage of grid nodes with RMS ≤5 mGal/km (%)	Percentage of grid nodes with RMS ≤10 mGal/km (%)
GEBCO	2.450 (0.086)	9.766 (3.246)	3.730	57.102
SIO V15.1	2.608 (0.144)	6.238 (1.445)	18.269	97.561
SIO V18.1	2.607 (0.126)	6.253 (1.661)	21.525	97.394
BAT_VGG	2.704 (0.139)	5.834 (1.572)	32.042	99.044

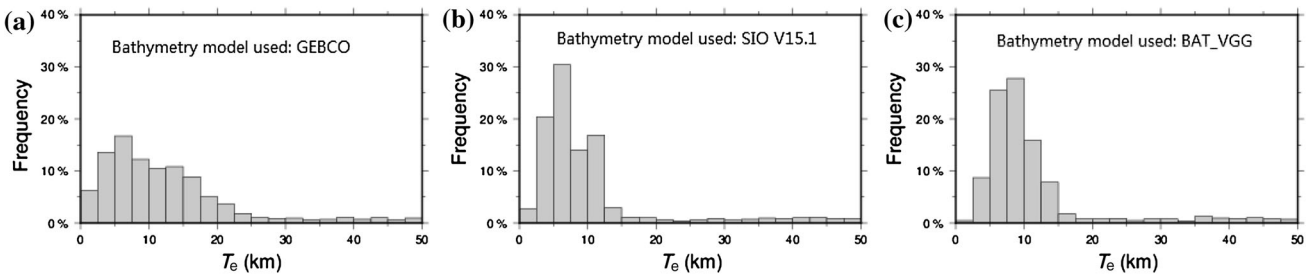

Fig. 6 Frequency distribution histograms of T_e over the Louisville Ridge and the adjacent regions for different bathymetry models: **a** GEBCO, **b** SIO V15.1, and **c** BAT_VGG

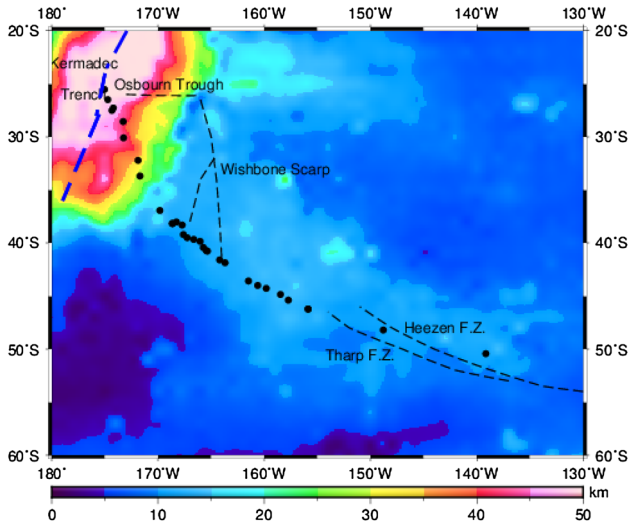

Fig. 7 T_e estimated using the bathymetry model BAT_VGG and the altimetric gravity anomalies from SIO V20.1 with the MWAT method. *Black dots* indicate locations where seamount ages are sampled

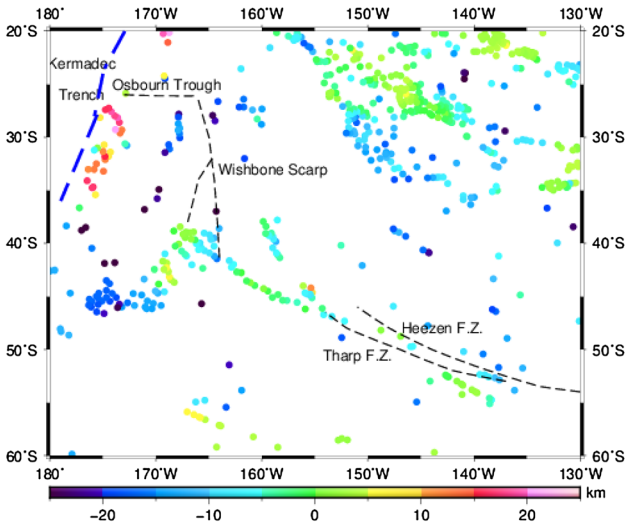

Fig. 8 Differences between the results for T_e at some seamounts from Watts et al. (2006) and the results from this study

Along the Louisville Ridge, T_e of the lithosphere was estimated by Cazenave and Dominh (1984), Watts et al. (1988), and Lyons et al. (2000). For comparison, the MWAT method is used here to calculate T_e of regions A-L of Lyons et al. (2000). The results are summarized in Table 4. According to Table 4 and Fig. 7, T_e along the Louisville Ridge is usually less than 15 km, except for the Kermadec outer rise, where it is larger than 20 km. This may due to the dynamic effect of plate subduction and the use of the wrong window size in the MWAT method. For profiles 1–4 in Watts et al. (1988), near the trench, if a $4° \times 4°$ window is used with the MWAT method, the best fitted T_e will be 10.5, 8.5, 10, and 13 km, respectively, which are consistent with the values of T_e given by Watts et al. In the southeast of the ridge, our results are consistent with those of Lyons et al. (2000). The values of T_e on the ridge show no trend like that in the Hawaiian-Emperor seamount chain.

5 Discussion and conclusions

Previous studies of oceanic lithospheric effective T_e suggest that the strength of the lithosphere under seamounts and islands depends strongly on the age at the time of loading (Watts 1978, 2001; Calmant et al. 1990). The precise relationship recovered between T_e and age at time of loading varies and there is no single isotherm that controls T_e on a global scale (Kalnins and Watts 2009). Within the study area, we have collected 33 sampled seamounts whose ages are known (Clouard and Bonneville 2005; Koppers et al. 2004, 2011). The values of T_e on these seamounts are interpolated from the T_e model shown in Fig. 7. Seafloor ages under these seamounts are interpolated from Müller et al. (2008). The locations of the sampled seamounts and the estimated values of T_e are collected in Table 5.

According to the plate cooling model (Parsons and Sclater 1977; Stein and Stein 1992), the lithosphere will get colder and stronger further away from the mid-ocean ridge. Many studies have suggested that the lithospheric T_e is to the first order determined by the age of lithosphere at the time of loading, and is given approximately by the depth to the 450 ± 150 °C isotherm (Watts 1978, 2001; Calmant et al. 1990).

Figure 9 shows the relationship between T_e and the age of the lithosphere at the time of loading over the Louisville Ridge. The relationships over the Hawaiian-Emperor Chain and the Line Seamounts are also given for comparison.

According to Fig. 9, in the study area, the dependence of T_e on the age of the oceanic lithosphere at the time of loading is given mostly by the depth to the 150 °C–300 °C isotherm based on a cooling plate model. The values of T_e over the Louisville Ridge are larger than those over the Line Ridge and lower than those over the Hawaiian-Emperor Chain. The T_e of the lithosphere does not increase with the age of the lithosphere at the time of loading. These results indicate that T_e is not controlled only by the age of the lithosphere at the time of loading. The eight samples in the northwest of the ridge show T_e larger than 20 km. We attribute this to the dynamic effects of plate subduction. The most significant topography loads are the islands arc at the west of the trench. These loads are supported by plate subduction. But, when we calculate T_e using MWAT method, it seems like these loads are supported

Table 4 Best fitting T_e from Cazenave and Dominh (1984), Watts et al. (1988), Lyons et al. (2000), and this study

Profiles	Watts et al.	Cazenave and Dominh, 2D	Cazenave and Dominh, 3D	Lyons et al. nonlinear	Lyons et al. linear	This study			Regions
						Lower	Best	Upper	
1	12.5–17.5		21.7–23.1	26.5	27	21	47.4[a]	50	A
2	10–20	15–20	18.6–21.4	24	24	7.5	30.1[a]	50	B
3	10–17			24	24				B
4	<15		12.8–18.8	23	23	9	15.1[a]	24	C
5	12.5–20			23	23				C
6	30–37.5			23.5	23	8	13.5	20	D
7				23.5	23				D
8	34–41	12–15	16.6–19	7	8	8	10.8	17	E
9				13.5	15.5	8	11.5	16	F1
10	27.5–32.5	10–12	16.6–17.8	13.5	15.5				F1
9				11.5	13				F2
10	27.5–32.5	10–12	16.6–17.8	11.5	13				F2
11	37.5–42.5	12–15	16.6–19	11	14	6	11	19	G
12	32.5–42.5	12–15	16.6–19	11	14				G
				15	15.5	9.5	13.4	20.5	H
				13	14.5	5.5	11.3	18	I2
				10	12				I3
				9.5	10	7.5	11.7	16	J
				9.5	9.5	6	12.9	18	K
				11.5	12	7	10.8	19	L

This table is modified from Table 1 of Lyons et al. (2000)

[a] If the window size is 4° × 4° when using the MWAT method to estimate T_e of profiles 1–4, the results will be 7.5–17, 7.5–10, 7.5–12.5, and 9–22.5 km, respectively, and the best fitted T_e will be 10.5, 8.5, 10 and 13 km. These results are consistent with those of Watts et al. (1988)

Table 5 Ages of seamounts and seafloor, and T_e estimated over the Louisville Ridge

Samples' name (Longitude, latitude)	Age of seamount (Ma)	Age of seafloor (Ma)	T_e (km)	References
Sotw9-58-1a/7 (184.96°, −25.53°)	77.75	86	50	Koppers et al. (2004)
U1372-Canopus (185.27°, −26.49°)	74	87	50	Koppers et al. (2012)
Sotw9-52-1 (185.79°, −27.28°)	68.9	89	48.3	Koppers et al. (2004)
AMAT-1D-1/3/5 (185.657°, −27.515°)	70.4	89	48.4	Koppers et al. (2011)
U1373/1374-Rigil (186.72°, −28.56°)	69 (67–71)	92	39.3	Koppers et al. (2012)
Sotw9-48-2 (186.75°, −30.1°)	61.4	98	42.9	Koppers et al. (2004)
U1376-Burton (188.12°, −32.22°)	64	104	27.7	Koppers et al. (2012)
U1375-Achernar (188.3°, −33.7°)	59	108	25.6	Koppers et al. (2012)
Vm5 (188.8°, −33.94°)	53.5	109	15	Clouard and Bonneville (2005)

Table 5 continued

Samples' name (Longitude, latitude)	Age of seamount (Ma)	Age of seafloor (Ma)	T_e (km)	References
Vm36-04 (190.167°, −36.95°)	46.3	121	13.7	Koppers et al. (2004)
AMAT-7D-1/3/6 (191.735°, −38.038°)	48.9	125	13.2	Koppers et al. (2011)
AMAT-10D-2/3/4 (191.34°, −38.172°)	49.9	125	13.2	Koppers et al. (2011)
U1377-Hadar (191.36°, −38.188°)	50	125	12.1	Koppers et al. (2012)
Vm36-03 (192.272°, −38.325°)	44.5	127	12.1	Koppers et al. (2004)
AMAT-14D-9/11 (192.382°, −39.218°)	44.3	129	10.1	Koppers et al. (2011)
AMAT-15D-1a (192.745°, −39.52°)	45.1	130	10.3	Koppers et al. (2011)
AMAT-16D-1 (193.357°, −39.677°)	43.3	131	10.9	Koppers et al. (2011)
AMAT-17D-1 (193.955°, −39.865°)	41.3	133	11	Koppers et al. (2011)
AMAT-20D-15B/17/3/8/9 (194.26°, −40.445°)	40.017	135	11	Koppers et al. (2011)
AMAT-22D-3/4 (194.54°, −40.742°)	39.25	136	11.3	Koppers et al. (2011)
Vm36-02 (194.65°, −40.783°)	33.9	136	11.6	Koppers et al. (2004)
VG-3a/MSN110-1 (195.8°, −41.613°)	36.5	108	11.1	Koppers et al. (2004)
AMAT-24D-2/3/6 (196.302°, −41.878°)	34.3	83	11.3	Koppers et al. (2011)
AMAT-26D-1/3/7/9 (198.512°, −43.575°)	30.667	77	12.4	Koppers et al. (2011)
AMAT-27D-1/7/13 (199.382°, −43.995°)	27.433	76	12.1	Koppers et al. (2011)
AMAT-28D-1 (200.185°, −44.275°)	25.6	74	14.4	Koppers et al. (2011)
AMAT-30D-7/8 (201.527°, −44.843°)	26.167	72	13.5	Koppers et al. (2011)
AMAT-31D-2/5/17 (202.267°, −45.382°)	24.367	71	13.2	Koppers et al. (2011)
AMAT-33D-1/2/3 (204.122°, −46.22°)	21.6	67	12.4	Koppers et al. (2011)
AMAT-32D-5 (204.12°, −46.227°)	21.3	67	12.8	Koppers et al. (2011)
MTHN-6D1 (211.2°, −48.2°)	13.2	60	10	Koppers et al. (2004)
MTHN-7D1 (220.85°, −50.433°)	1.112	46	9.9	Koppers et al. (2004)

The ages of the seamounts are taken from the references. The age of the seafloor is interpolated from Müller et al. (2008). T_e is estimated in this study

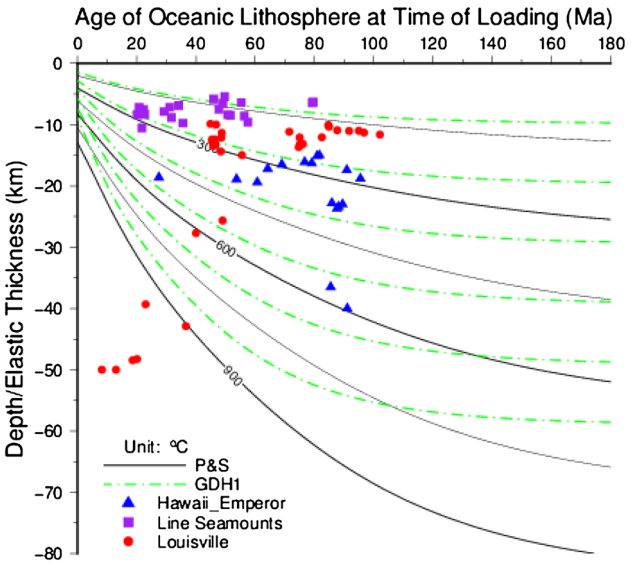

Fig. 9 T_e versus the age of the oceanic lithosphere at the time of loading. *Lines P&S* and *GDH1* represent the cooling plate models given by Parsons and Sclater (1977) and Stein and Stein (1992), respectively, *blue triangles*, *red circles*, and *purple squares* denote seamounts on the Hawaiian-Emperor Chain, the Louisville Ridge, and the Line Seamounts, respectively. The values of T_e over the Hawaiian-Emperor Chain and the Line Seamounts were calculated by the authors using the same data and method as in this paper

by the strength of lithosphere. Therefore, we must be careful if the MWAT method is used to calculate the T_e of the trench outer rise.

Acknowledgments This study was supported financially by the Key Foundation of the Institute of Seismology, China Earthquake Administration (No. IS201506205), and the National Natural Science Foundation of China (Nos. 41504017, 41204019, 41304003). We also want to say thank you to the reviewers for their useful comments.

References

Calmant S, Francheteau J, Cazenave A (1990) Elastic layer thickening with age of the oceanic lithosphere: a tool for prediction of the age of volcanoes or oceanic crust. Geophys J 100:59–67

Cazenave A, Dominh K (1984) Geoid heights over the Louisville Ridge (South Pacific). J Geophys Res 89:11171–11179

Clouard V, Bonneville A (2005) Ages of seamounts, islands and plateaus on the Pacific Plate. In: Foulger GR, Natland JH, Presnal D, Anderson DL (eds) Plates, plumes and paradigms (Special paper), vol 388. Geological Society of America, pp 71-90

Hu MZ, Li JC, Li H, Shen CY, Jin TY, Xing LL (2014) Predicting global seafloor topography using multi-source data. Mar Geod. doi:10.1080/01490419.2014.934415

Kalnins LM, Watts AB (2009) Spatial variations in effective elastic thickness in the western Pacific Ocean and their implications for Mesozoic volcanism. Earth Planet Sci Lett 286:89–100

Koppers AAP, Duncan RA, Steinberger B (2004) Implications of a nonlinear $^{40}Ar/^{39}Ar$ age progression along the Louisville seamount trail for models of fixed and moving hot spots. Geochem Geophys Geosyst 5:Q06L02. doi:10.1029/2003GC000671

Koppers AAP, Gowen MD, Colwell LE, Gee JS, Lonsdale PF, Mahoney JJ, Duncan RA (2011) New $^{40}Ar/^{39}Ar$ age progression for the Louisville hot spot trail and implications for inter-hot spot motion. Geochem Geophys Geosyst 12:Q0AM02. doi:10.1029/2011GC003804

Koppers AAP, Yamazaki, T, Geldmacher J (eds), IODP Expedition 330 Scientists (2012) Louisville Seamount Trail: Expedition 330 of the riserless drilling platform from and to Auckland, New Zealand, Sites U1372–U1377, 13 December 2010–11 February 2011, Proceedings of the Integrated Ocean Drilling Program, 330

Luis JF, Neves MC (2006) The isostatic compensation of Azores Plateau: a 3D admittance and coherence analysis. J Volcanol Geotherm Res 156:10–22

Lyons SN, Sandwell DT, Smith WHF (2000) Three-dimensional estimation of elastic thickness under the Louisville Ridge. J Geophys Res 105(B6):13239–13252

Marks KM, Smith WHF (2006) An evaluation of publicly available global bathymetry grids. Mar Geophys Res 27:19–34

McNutt M (1979) Compensation of oceanic topography: an application of the response function technique to surveyor area. J Geophys Res 84:7589–7598

Müller RD, Sdrolias M, Gaina C, Roest WR (2008) Age, spreading rates, and spreading asymmetry of the world's ocean crust. Geochem Geophys Geosyst 9(4):1–19

Parker RL (1973) The rapid calculation of potential anomalies. Geophys J R Astron Soc 31:447–455

Parsons B, Sclater JG (1977) An analysis of the variation of ocean floor bathymetry and heat flow with age. J Geophys Res 82(5):803–827

Sandwell DT, Smith WHF (2009) Global marine gravity from retracked Geosat and ERS-1 altimetry: ridge segmentation versus spreading rate. J Geophys Res. doi:10.1029/2008JB006008

Smith WHF (1993) On the accuracy of digital bathymetric data. J Geophys Res 98(86):9591–9603

Smith WHF, Sandwell DT (1994) Bathymetric prediction from dense satellite altimetry and sparse shipboard bathymetry. J Geophys Res 99:21803–21824

Stein CA, Stein S (1992) A model for the global variation in oceanic depth and heat flow with lithospheric age. Nature 359:123–129

Walcott RI (1976) Lithospheric flexure, analysis of gravity anomalies, and the propagation of seamount chains. In: Sutton GH, Manghnani MH, Moberly R (eds) The geophysics of the Pacific Ocean Basin and its margin. Geophysical monograph, 19. American Geophysical Union, Washington, DC, pp 431–438

Watts AB (1978) An analysis of isostasy in the world's oceans: 1 Hawaiian-Emperor seamount chain. J Geophys Res 83(B12):5989–6004

Watts AB. 2001. Isostasy and Flexure of the Lithosphere. Cambridge University Press, Chapter5

Watts AB, Weissel JK, Duncan RA, Larson RL (1988) Origin of the Louisville Ridge and its relationship to the Eltanin fracture zone system. J Geophys Res 93(B4):3051–3077

Watts AB, Sandwell DT, Smith WHF, Wessel P (2006) Global gravity, bathymetry, and the distribution of submarine volcanism through space and time. J Geophys Res. doi:10.1029/2005JB004083

Wessel P, Harada Y, Kroenke L (2006) Toward a self consistent, high-resolution absolute plate motion model for the Pacific. Geochem Geophys Geosyst 7:Q03L12. doi:10.1029/2005GC001000